

# Optical properties determined from infrared spectroscopy and structural properties from diffraction spectroscopy of composites Fe/CNs/PVA for electromagnetic wave absorption

Yulia Kirana Lahsmin, Heryanto Heryanto, Sultan Ilyas, Ahmad Nurul Fahri, Bualkar Abdullah, Dahlang Tahir\*

Department of Physics, Hasanuddin University, Makassar, 90245, Indonesia

## ARTICLE INFO

### Keywords:

XRD  
FTIR  
VNA  
Optical properties  
Working frequency  
Reflection loss

## ABSTRACT

Structural, optical, and absorption properties of nano-composites iron powder/carbon nano-sphere/polyvinyl alcohol (Fe/CNs/PVA) for electromagnetic (EM) wave absorber based on CNs from bamboo fiber studied by X-ray diffraction (XRD), Fourier transforms infra-red (FTIR), and vector network analyzer (VNA), respectively. The existence of the diffraction peaks identified by crystal orientation (hkl) (004), (224) and (115) with FWHM, strain, and working frequency increases with increasing the activation temperature indicated the formation of the new structures. These findings consistent with the distance ( $\Delta(\text{LO-TO})$ ) between two optical phonon vibrations mode increases indicated that, the stable covalent bonding formation of Fe/CNs/PVA particles increase with increasing the temperature activation of CNs. Temperature activation of the CNs play an important role in expanding the frequency up to 5.56 GHz with reflection loss (RL)  $-23.16$  dB, indicated that a new type absorber for attenuating 99% EM wave. This study shows that the FTIR spectra could be useful for determining the optical properties, phonon vibration, dielectric function, and energy loss function of composite Fe/CNs/PVA.

## 1. Introduction

The development of modern technology has succeeded in creating sophisticated electronic devices and telecommunications systems, contributing to increasing the electromagnetic (EM) radiation [1–11]. The EM radiation in the environment resulted in the crosstalk or inter-modulation in the form of electromagnetic interference (EMI). For reducing the EMI problem, the scientist in the world has attracted the attention of looking at the new absorber of EM wave with broad absorption frequency [1,2,7,9–12]. The effort to produce the EM wave absorber is not only by paying attention to the lightweight and excellent absorber properties but also by thin [1,3,7,9–14].

Generally, microwave absorber materials are classifying into two categories: dielectric loss material and magnetic loss material based on their mechanism and function in absorbing the EM wave [1,15–17]. Single dielectric or magnetic materials are usually incapable due to the high impedance that causes the poor to absorb EM waves [2–4,8]. Ref. [1–6,9,18,19] reported that the iron is a material with excellent magnetic characteristics for absorber of EMI but should be combining

with other materials to form the composite. The additional organic matter, such as carbon in the form of composite, could be useful for increasing the absorption performance of EMI [1,3,4,7,9–11]. Composite iron-carbon shows the stability of the chemical bonds [1,4,8,9], low density [10,11,20], the surface of the electron interactions is broad [7,9]. Some references also used activated carbon [1,7,9–11], stacked porous carbon nanosheets [21], porous carbon network [22], biomass reinforced [23], Co/C composite [24], and carbon nano-sphere [13,14], which used to stabilize the structure of metal oxides and avoid the formation of unstable bonding between the atoms on the surface and interface of the composite [1,9,11]. High-frequency absorption and also stable performance in absorbing EM waves of new type's nano-composites are still challenges. The utilization of CNs for attachment of iron particles high potentials for reducing the magnetic properties and increasing the absorption frequency [1,5]. Applying the temperature treatment in the activation of CNs could be useful for reducing the unstable bonding at the surface, which contributed to expanding the absorption of EM waves. By using CNs, the electromagnetic wave absorption performance improves [13,14], which is probably due to the

\* Corresponding author.

E-mail address: [dtahir@fmipa.unhas.ac.id](mailto:dtahir@fmipa.unhas.ac.id) (D. Tahir).

<https://doi.org/10.1016/j.optmat.2020.110639>

Received 28 August 2020; Received in revised form 30 September 2020; Accepted 9 November 2020

0925-3467/© 2020 Elsevier B.V. All rights reserved.

dipole relaxation, and also the stable bonding between the atoms at the surface is increasing [1,7].

The carbon nano-spheres (CNs) are synthesized from bamboo fibers using the simple method described in detail in our previous study in Ref. [25] with average particle size is 23 nm which determined from the transmission electron microscope (TEM) image. The activation temperature of carbon nano-spheres was varied for increasing the stable bonding at the surface, which was useful for increasing the EMI absorption performance. The effect of activation temperature of CNs on the structural, optical, and absorption properties as the fundamental knowledge to understand the mechanism and the relation between these properties in supporting the performance of the nanocomposites Fe/CNs/PVA has not experimentally investigated adequately. The CNs from the bamboo fibers are high potential for using a matrix to attach the Fe particles and reduce the magnetic properties of nanocomposites Fe/CNs/PVA. In this study, by applying Kramers Kronig (KK) relation in the quantitative analysis of the FTIR spectra, the optical properties in the form of the refractive index ( $n$ ) and extinction coefficient ( $k$ ) determined and then continue to find the dielectric function ( $\epsilon$ ) and energy loss function ( $\text{Im}(-1/\epsilon)$ ). XRD spectra used for the analysis of structural properties and VNA used to determine the absorption properties in the form of reflection loss (RL) and the working frequency of nanocomposite Fe/CNs/PVA. From an analysis of the optical properties, the longitudinal (LO) and transversal (TO) optical phonon vibration identified. The relation between structural and optical properties to the RL and working frequency of nanocomposites Fe/CNs/PVA for various CNs activation temperatures used to find the best characteristic in supporting the composite material performance.

## 2. Experiment

### 2.1. Materials

Carbon nanosphere (CNs) is synthesized from bamboo fiber as reported in our previous study in Ref. [25], Polyvinyl Alcohol (99.5% PVA, Merck), Iron Powder (Fe) was purchased from Sigma-Aldrich in a form of carbonyl-iron powder, low in magnesium and manganese compounds,  $\leq 99.5\%$ , resistivity  $9.71 \mu\Omega\text{cm}$ , impurities  $\leq 0.01\%$  total Nitrogen (N) and grain size  $5-9 \mu\text{m}$  [1]. Aquades (H<sub>2</sub>O, Merck).

### 2.2. Sample preparation

The carbon nano-spheres (CNs) are synthesized from bamboo fibers using the simple method, for the activation temperatures: (A) 105 °C, (B) 155 °C, (C) 205 °C, (D) 255 °C and (E) 305 °C. We found the average particle size is 23 nm by transmission electron microscope (TEM), for more detail about synthesis and activation processes was described in detail in our previous study [25]. About 15% of CNs taken for each activation temperature with the total amount of CNs + Fe is 15 g for homogenized using Mixing MM Retsch at the frequency of 10 Hz for 30 min. The homogeneous sample is putting in a cup, added 5 ml PVA 2%, and then stirred for 30 min at the temperature 50 °C and constant speed 600 rpm. After samples became slurry, the samples were pelleting with a thickness of 2 mm, 3 mm, and 4 mm for each composition using a hydraulic compactor with a pressure 50 kPa for 5–7 min. The pellet samples were heating by using a furnace at 80 °C for 5 h. The illustration synthesis process of nano-composites pellets for the absorber of EM waves in this study is in Fig. 1.

### 2.3. Sample characterization

Samples were characterized to determine the ability of wave absorption using Vector Network Analyzer (VNA) (Rohde & Schwarz, ZVHB) with a frequency range from 3.5 GHz to 8 GHz [1]. The chemical bonds from the functional groups and the optical properties of the nano-composite Fe/CNs/PVA were analysis from the Fourier transform

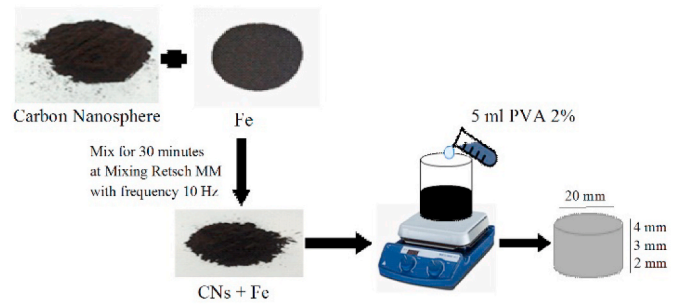


Fig. 1. The schematic diagram of synthesis nanocomposites Fe/CNs/PVA for the absorber of EM waves application.

infrared (FTIR) spectra (IRPrestige-21 FTIR spectrometer (Shimadzu Corp)) and the structural properties by X-ray diffraction (XRD) (Shimadzu 7000) with radiation  $\text{CuK}\alpha$  ( $\lambda = 1.5405 \text{ \AA}$ ) angular range  $20^\circ \leq 2\theta \leq 60^\circ$ , which is operated at 30 kV and 10 mA.

## 3. Results and discussion

### 3.1. XRD analysis

Fig. 2 shows the XRD spectra (a) for full spectra, (b) for diffraction peak at (110), and (c) for (114) of nano-composites Fe/CNs/PVA for various activation temperatures of CNs; 105 °C, 155 °C, 205 °C, 255 °C, and 305 °C for  $2\theta$  from  $20^\circ$  to  $60^\circ$ . The crystalline phase is formed at crystal orientations (hkl) peaks: (002), (104), (110), (004), (224) and (115) based on the previous studies for CNs [25]. Peaks (002) indicate the miller index of hexagonal graphite structure [1], crystal orientations (hkl) peaks: (104) and (110) from Fe [1]. Based on Fig. 2 (c), it can be seen that for  $2\theta$  at  $56.8^\circ$  there is still a carbon crystal phase in the CNs for the activation temperature 105 °C. By the increasing, the activation temperature indicated (B), (C), (D), and (E) in Fig. 2 (a) respectively for 155 °C, 205 °C, 255 °C, and 305 °C shows the crystalline phase shifts towards amorphous phase (for more clearly see Fig. 2 (c), for diffraction peak (114) which is a good characteristic for reducing magnetic properties [5,6,16]. For crystal orientations (hkl) at (004), (224) and (115) are indicated the new bonding connection between CNs-Fe-PVA particles [1,25]. The average crystallite size (see Table 1) is around

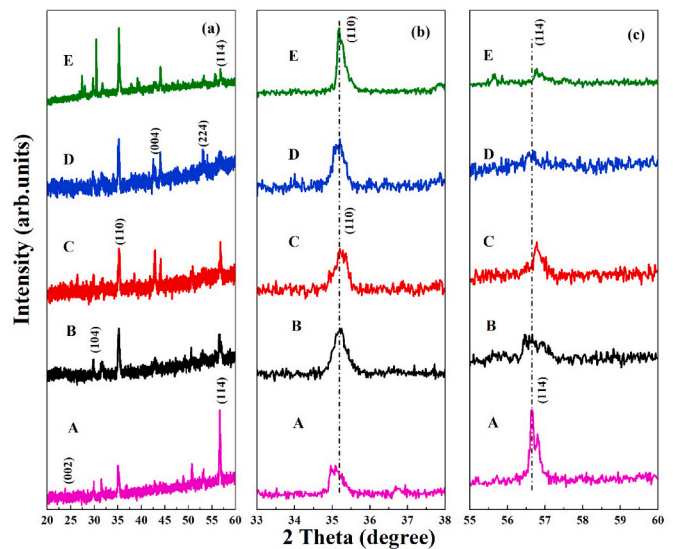


Fig. 2. XRD spectra of nanocomposites Fe/CNs/PVA with CNs at activation temperature (A) 105 °C, (B) 155 °C, (C) 205 °C, (D) 255 °C and (E) 305 °C. (a) for full spectra, (b) diffraction peak for (110), and (c) for (114).

**Table 1**

Crystallite size, dislocation density, LO, TO, and ( $\Delta=(LO-TO)$ ) from the quantitative analysis of XRD spectra in Fig. 2 for nanocomposites Fe/CNs/PVA with CNs with activation temperature was varied; (A) 105 °C, (B) 155 °C, (C) 205 °C, (D) 255 °C and (E) 305 °C.

Sample ID	Crystallite size (nm)	Dislocation density ( $\text{nm}^{-2}$ )	LO ( $\text{cm}^{-1}$ )	TO ( $\text{cm}^{-1}$ )	$\Delta(LO-TO)$ ( $\text{cm}^{-1}$ )
(A)	42.31	0.0006	665	565	100
(B)	20.35	0.0024	673	560	113
(C)	49.70	0.0004	657	570	87
(D)	18.97	0.0028	654	570	84
(E)	29.02	0.0019	680	560	120

9–15 nm which was calculated by using the Scherrer equation [16]:

$$L_c = \frac{K\lambda}{\beta \cos \theta} \quad (1)$$

where  $L_c$  is the average crystal size (nm);  $K$  is the Scherrer parameter that was taken to be 0.89;  $\lambda$  is 1.54056 nm for Cu is the source of the radiation, and  $\beta$  is the full width half maximum (FWHM) in radians. The dislocation density ( $\delta$ ) (see Table 1) calculated by the following equation [7]:

$$\delta = \frac{1}{L_c^2} \quad (2)$$

Fig. 3 shows the relationship between the FWHM and the strains of nanocomposites Fe/CNs/PVA for the activation temperature was varied 105 °C, 155 °C, 205 °C, 255 °C, and 305 °C. By increasing the activation temperature shows strongly influenced the FWHM and the strain value, the new structures formed [3,11,16,20]. Fig. 2 of the XRD spectra confirm that the new structure formation indicated by the new peaks increases as the temperature increases. For small FWHM values strongly correlated with granules of CNs with fewer defects [9,13] and by the increase of the strain value, and the dislocation density indicates the amount of the defect due to the breaking bond between the atoms or by missing the atoms in the arrangement is increased. The defect will create pore, which leads to a decrease in mechanical properties. The crystallite size determined from the analysis of the XRD spectra in Fig. 2 by using eq. (1) and the dislocation density by eq. (2) are shown in Table 1.

### 3.2. FTIR analysis

Fig. 4 shows FTIR spectrum of nanocomposite Fe/CNs/PVA for an activation temperature of CNs was varied as indicated in the figure by

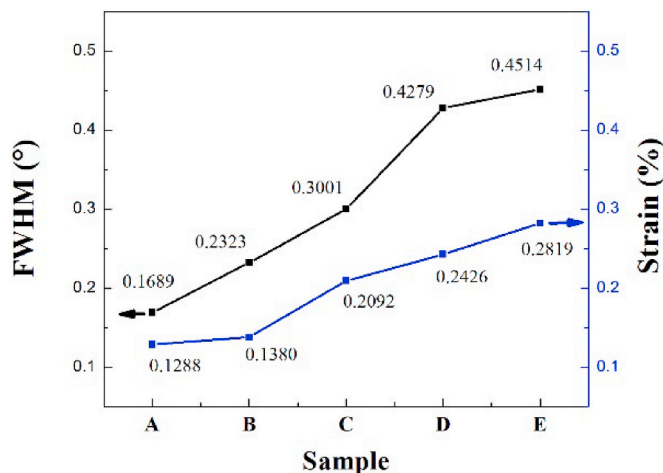


**Fig. 3.** FWHM and strain values from the quantitative analysis of XRD spectrum of Fe/CNs/PVA nanocomposites for various activation temperature: (A) 105 °C, (B) 155 °C, (C) 205 °C, (D) 255 °C and (E) 305 °C.

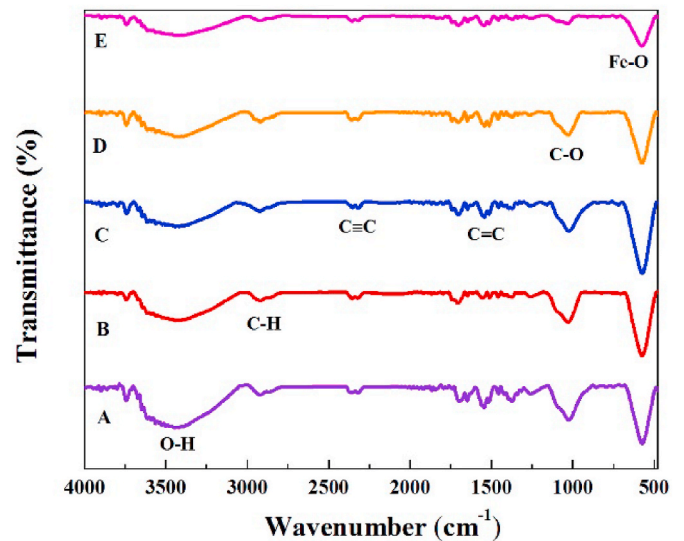


**Fig. 4.** FTIR spectra of nanocomposite Fe/CNs/PVA with CNs at activation temperature (A) 105 °C, (B) 155 °C, (C) 205 °C, (D) 255 °C and (E) 305 °C.

(A) 105 °C, (B) 155 °C, (C) 205 °C, (D) 255 °C and (E) 305 °C at the wavelength in between 500 and 4000  $\text{cm}^{-1}$ . It can be seen in Fig. 4 that carbon with an activation temperature increase from 105 °C to 305 °C forming O–H, C–H, C≡C, C=C, C–O and Fe–O bond. At the wavelength 3429  $\text{cm}^{-1}$  is O–H bond which is a hydrogen bond in alcohol compound, C–H bond at the wavelength 2918  $\text{cm}^{-1}$  is an alkane compound, C≡C and C=C bond at the wavelength 2343  $\text{cm}^{-1}$  and 1544  $\text{cm}^{-1}$  is contributed from CNs. For the wavelength 1027  $\text{cm}^{-1}$  is C–O bond. Bonding of compounds at the wavelength 1027  $\text{cm}^{-1}$  to the wavelength 3429  $\text{cm}^{-1}$  is a bonding in the CNs that has been synthesized from bamboo fiber [25] and at the wavelength 575  $\text{cm}^{-1}$  is Fe–O bonds which were the intensity decrease with increasing the activated temperature of the nano-sphere is may due to the phase change from crystal to the amorphous phase of carbon [25]. For activation of CNs at high temperatures shows the dominant amorphous phase which facilitates the Fe atom attaches on CNs by covalent bonds [1]. The intensity of the C=C bond at a wavelength of 1544  $\text{cm}^{-1}$  changes from width to narrow after being formed into nanocomposites Fe/CNs/PVA due to the structural properties changed. The C–O bond at wavelength 1027  $\text{cm}^{-1}$  is a compound type of alcohol group which plays a role in increasing the dispersion of PVA, where PVA acts as binders on nanocomposites materials forming uniform bonding between CNs and Fe particles. It is indicated that the nanocomposite Fe/CNs/PVA in this study produces a better magnetic network to reflect EM waves [1,7,9]. The PVA can increase the dielectric losses due to the dipole relaxation and the interface relaxation [8,17]. PVA's amorphous nature in composite Fe/CNs/PVA facilitates the rotational motion of (O–H and C–O) dipolar group attached to polymers as a side-chain dipole. Ref. [26,27] reported three dipole relaxation processes: first, at low frequency, is associated with the rotation of the functional group around the main chain axis. Second, at middle frequency is the result of the orientation of polar functional group O–H or C–O existing in PVA's side chain. The third is dipole relaxation at high frequency due to the rotational motion of the polar functional (O–H) attached to the PVA's side chain. For the amorphous phase, the interfacial and dipole relaxation are enhancing, which would significantly increase the dielectric permittivity and relatively low dielectric losses, consequently increasing microwave absorption. The optical properties, dielectric function, and the energy loss function can be derived from the quantitative analysis of electron spectroscopy spectra [7,9,19,28–33] and from the infra-red spectroscopy [34–36] as used in this study by applying Kramers Kronig (KK) relation. The optical properties in the form of the refractive index ( $n$ ) and extinction

coefficient ( $k$ ), the dielectric function in the form of the real part ( $\epsilon_1(\omega)$ ) and the imaginary part ( $\epsilon_2(\omega)$ ), and the energy loss function  $\text{Im}(-1/\epsilon_1(\omega))$ . For these purposes, the FTIR spectra converted from the transmittance spectra to the reflectance spectra as follows [34,37,38]:

$$A(\omega) = 2 - \log[T(\omega)\%] \quad (3)$$

$$R(\omega) = 100 - [T(\omega) + A(\omega)] \quad (4)$$

The refractive index  $n(\omega)$  is for the real part and the extinction coefficient  $k(\omega)$  is for the imaginary part [34–38]:

$$n(\omega) = \frac{1 - R(\omega)}{1 + R(\omega) - 2\sqrt{R(\omega)}\cos\phi(\omega)} \quad (5)$$

$$k(\omega) = \frac{2\sqrt{R(\omega)}\sin\phi(\omega)}{1 + R(\omega) - 2\sqrt{R(\omega)}\cos\phi(\omega)} \quad (6)$$

where  $\phi(\omega)$  is the phase change between for the photon signals from the incident to the reflection after passing through the FTIR spectroscopy system described by the equation as follows:

$$\phi(\omega) = -\frac{\omega}{\pi} \int_0^{\infty} \frac{\ln R(\omega') - \ln R(\omega)}{\omega'^2 - \omega^2} \quad (7)$$

by applying K-K relation, equation (7) become:

$$\phi(\omega_j) = -\frac{4\omega_j}{\pi} \Delta\omega \sum_i \frac{\ln(\sqrt{R(\omega_i)})}{\omega_i^2 - \omega_j^2} \quad (8)$$

$j$  is a series of wavenumber, if  $j$  is an odd number so then  $i$  parts is 2,4,6,8, ...,  $j-1, j+1$  and while wavenumber  $j$  is an even,  $i$  parts is 1,3,5,7, ...,  $j-1, j+1, \dots$   $\Delta\omega = \omega_{i+1} - \omega_i$ . The intersection point of  $n$  and  $k$  related to the optical intersection with the lattice indicated by the dotted line in Fig. 5 for transverse optical (TO) phonon mode at the lower wavelength and longitudinal optical (LO) phonon vibration at a higher wavelength. The distance between two optical phonon mode ( $\Delta(\text{LO-TO})$ ) shows shorter at the activation temperature 255 °C and the longer at 305 °C. The closer distance ( $\Delta$ ) at the temperature 205 °C and 255 °C are due to the non-uniformity lattice and less stable structure effect of cohesion force between Fe and CNs in the composite [34,38,39].

Dielectric function in the form of the real part  $\epsilon_1(\omega)$  and imaginary part  $i\epsilon_2(\omega)$  determined from the relations, respectively, as follows:

$$\epsilon_1(\omega) = n^2(\omega) - k^2(\omega) \quad (9)$$

$$\epsilon_2(\omega) = 2n(\omega)k(\omega) \quad (10)$$

Real ( $\epsilon_1(\omega)$ ) and imaginary part ( $\epsilon_2(\omega)$ ) of dielectric function are shown in Fig. 5 (middle). These peaks are mainly in the range from 520  $\text{cm}^{-1}$  to 570  $\text{cm}^{-1}$ . The optical properties change with the change the temperature in nanocomposite may due to the atomic bonding still adjusted and rearranged to form stable bonding with a new structure [34,40,41]. The stable bonding formation between Fe and CNs as a filler shows at the higher temperature indicated by the distance between two optical phonon modes ( $\Delta(\text{LO-TO})$ ) is higher.

Table 1 shows the LO and TO positions taken from Fig. 5 (top), and the distance ( $\Delta$ ) between two optical phonon modes. The TO and LO modes can be identified also from the main peak of the imaginary part ( $\epsilon_2(\omega)$ ) of the dielectric function in Fig. 5 (middle) and the energy loss function ( $\text{Im}(-1/\epsilon_1(\omega)) = (\epsilon_1(\omega))/(\epsilon_1^2(\omega) + \epsilon_2^2(\omega))$ ) in Fig. 5 (bottom), respectively. The energy loss function usually the same as the plasma frequency as reported in Refs. [7,9,19,28–33]. The detail wavenumber of LO, TO, and ( $\Delta = (\text{LO-TO})$ ) of nanocomposite in this study clearly shown in Table 1.

### 3.3. VNA analysis

Fig. 6 shows the absorption of electromagnetic waves on nanocomposite pellets using VNA in the frequency range from 3.5 GHz to 8 GHz. In this study, the effect of temperatures on the reflection loss (dB), frequency (GHz), and bandwidth for various thickness can be seen clearly in Table 2. Table 2 shows the highest RL for the higher activation temperature of CNs. Samples with a thickness of 2 mm show working frequencies from 5.21 GHz to 5.26 GHz. For 3 mm, the working frequency has decreased to 4.70 GHz; for 305 °C, it reaches the working frequency of 5.56 GHz, which is similar for all different thicknesses. Sample with a thickness 3 mm has RL from -18.78 dB to -23.16 dB, for 4 mm, at temperature 105 °C has RL -18.61 dB with working frequency 4.68 GHz and the highest RL is -23.64 dB for 305 °C with working frequency 5.09 GHz. Thus, the highest RL of these three samples found in samples with a thickness of 4 mm for activation temperature 305 °C. It indicates that the thickness is an essential parameter for increasing the reflection loss and the electromagnetic waves absorption level, which may indicate the stability of the structure and the bonding formation for new types of materials in the absorption of EMI. It can also see the effect of activation temperature in increasing the FWHM and the strain in the composite, which may directly correlate to increasing the absorption of EMI. The working frequency for all nanocomposites in this study shows the potential to attenuate 90% of EM wave due to the RL value less than

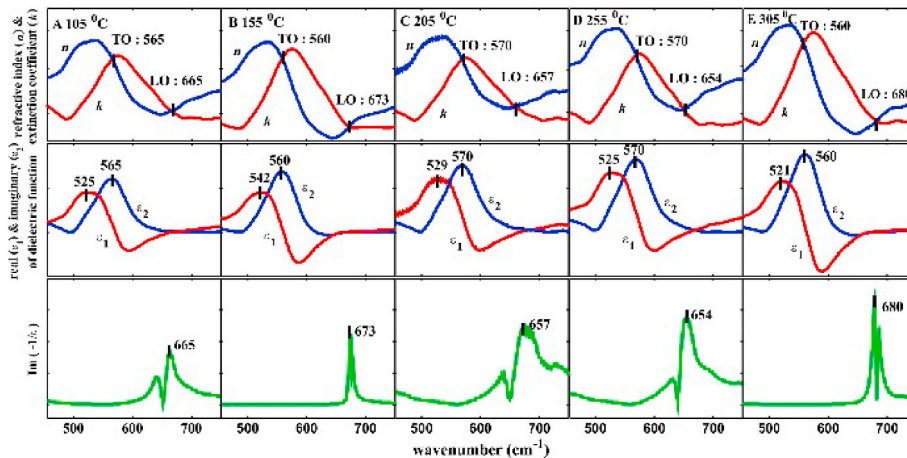


Fig. 5. The refractive index and the extinction coefficient (top row), the real and imaginary dielectric function (middle row) derived from the quantitative analysis of FTIR spectra in Fig. 4 and the energy loss function  $\text{Im}(-1/\epsilon_1(\omega))$  (bottom row) derived from the dielectric function for nanocomposite Fe/CNs/PVA as a function of activation temperature of CNs. The optical phonon vibration mode indicated by TO for transversal optical and LO for longitudinal optical.

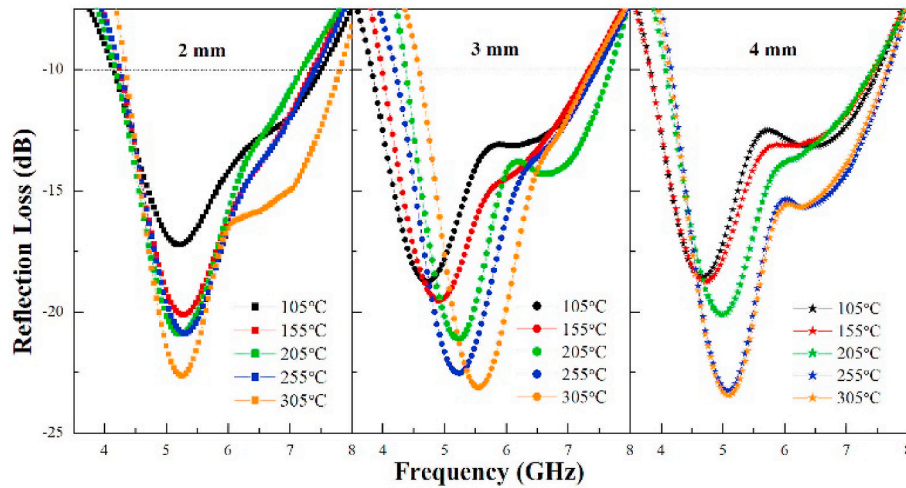


Fig. 6. Absorption of EM waves with activation temperatures of CNs (A) 105 °C, (B) 155 °C, (C) 205 °C, (D) 255 °C and (E) 305 °C in the thickness of pellets: 2 mm, 3 mm and 4 mm.

Table 2

The absorption of EM waves characteristics for the activation temperatures of CNs was varied 105 °C, 155 °C, 205 °C, 255 °C, and 305 °C and also the thickness of pellets was varied 1 mm, 2 mm, and 3 mm.

Thickness (mm)	Activation Temperature of CNs	Reflection loss (dB)	Working Frequency (GHz)	Frequency Bandwidth (GHz)
2	105 °C	-17.38	5.21	3.44
	155 °C	-20.29	5.27	3.11
	205 °C	-21.05	5.23	3.08
	255 °C	-21.05	5.32	3.13
	305 °C	-22.85	5.26	3.46
3	105 °C	-18.78	4.70	3.69
	155 °C	-19.65	4.90	3.21
	205 °C	-21.28	5.23	3.25
	255 °C	-22.73	5.25	3.24
	305 °C	-23.16	5.56	2.74
4	105 °C	-18.61	4.68	3.73
	155 °C	-18.91	4.71	3.63
	205 °C	-20.24	5.01	3.37
	255 °C	-23.35	5.09	3.49
	305 °C	-23.64	5.09	3.52

-10 dB and the potential to attenuate 99% for RL value less than -20 dB [1,7,9-14]. By using CNs the working frequency of nano-composites Fe/CNs/PVA in absorbing EM waves increased to 5.56 GHz, which were higher than the previous studies by using nanocomposite Fe/Activated Carbon/PVA about 4.65 GHz (see Fig. 6 for more detail) [1]. We have compared the working frequency and the reflection loss (RL) to shows novelty in this study with previously reported reference for different kinds of materials [42-57], see Table 3 for more details. The absorber using composite MWNT/SiO<sub>2</sub> and SiC<sub>f</sub>/Si<sub>3</sub>N<sub>4</sub> synthesized at high temperature (600 °C) with RL is -14 dB and -13 dB, respectively [55,56], indicated that, best results in this study. The type of carbon also influences the absorption properties, for CNT/SiO<sub>2</sub> at 500 °C shows RL -39.42 dB [57]. All these reported materials are used high technology in the preparations different in this study by simple methods. In this study, for activation at high temperature, the structure of CNs probably changes to the amorphous phase, which allows Fe attach on CNs network by covalent bonds [13,14]. More thickness may increase the covalent bonds between Fe and CNs, which is useful for reducing the magnetic properties. It can see from the working frequency of the previous study of nanocomposite Fe/AC/PVA is 4.65 GHz [1] and by using nanocomposite based CNs in this study, the working frequency was increased to 5.56 GHz.

Table 3

The electromagnetic absorption properties (working frequency and reflection loss) in this study by using bamboo fiber for activation temperature is 305 °C. We have included the different kind of materials from different references for comparison.

Material	Frequency (GHz)	Reflection loss (dB)	Reference
5% B and 15% N doped SiC	9.3	-7.6	[42]
0.5 TiO <sub>2</sub> + 1.5 Ni <sub>0.53</sub> Cu <sub>0.12</sub> Zn <sub>0.35</sub> Fe <sub>2</sub> O <sub>4</sub>	10.26	-28	[43]
Graphene oxide	13.1	-34	[44]
Graphene@PANI@Porous TiO <sub>2</sub>	11.5	-45.4	[45]
Fe <sub>3</sub> O <sub>4</sub> -rGO-PDMS	5.7	-50.5	[46]
Fe <sub>3</sub> O <sub>4</sub> /Graphene	11	-53.2	[47]
ZnO/Graphene	5.2	-52	[48]
Graphene/Carbon	5.7	-28.1	[49]
Epoxy-PPY/Fe <sub>3</sub> O <sub>4</sub> -ZnO	9.96	-32.53	[50]
Ti <sub>3</sub> C <sub>2</sub>	12.4	-11	[51]
Nitrogen-doped Graphene	12.7	-11.3	[52]
GNS@CoFe <sub>2</sub> O <sub>4</sub> /CNT aerogel	10.34	-29.1	[53]
Co NPs/Porous C	11.03	-30.31	[54]
MWNT/SiO <sub>2</sub> (600 °C)	~10.0	-14	[55]
MWNT/SiO <sub>2</sub> (30 °C)	~10.0	-20	[56]
SiC <sub>f</sub> /Si <sub>3</sub> N <sub>4</sub> (600 °C)	~12.5	-13	[57]
SiC <sub>f</sub> /Si <sub>3</sub> N <sub>4</sub> (25 °C)	~14.0	-13	
CNTs/SiO <sub>2</sub> (500 °C)	~10.0	-39.42	
CNTs/SiO <sub>2</sub> (100 °C)	~10.0	-30.72	
Bamboo fiber/Fe (305 °C)	5.09	-23.64	Present study

The relationship between activation temperature with the FWHM, strain, and working frequency for difference thickness (2 mm, 3 mm, and 4 mm) of the composite shown in Fig. 7. As can be seen clearly, the trend is similar between FWHM, strain, and working frequency increases with increasing the activation temperature indicate the formation of the new structures in the nano-composite reported in Refs. [30,40,41]. Similar to the distance ( $\Delta(\text{LO-TO})$ ) between two optical phonon vibrations is higher for the higher temperature indicated stable covalent bonding formation with a new structure was formed in composites [34, 38,39]. These properties are useful in supporting in increasing the absorption properties and working frequency indicated by the highest RL is -23.64 dB for 305 °C, which potential to attenuate 99% of EM wave for the working frequency 5.09 GHz.

#### 4. Conclusion

Nano-composite Fe/CNs/PVA has been synthesized by a simple

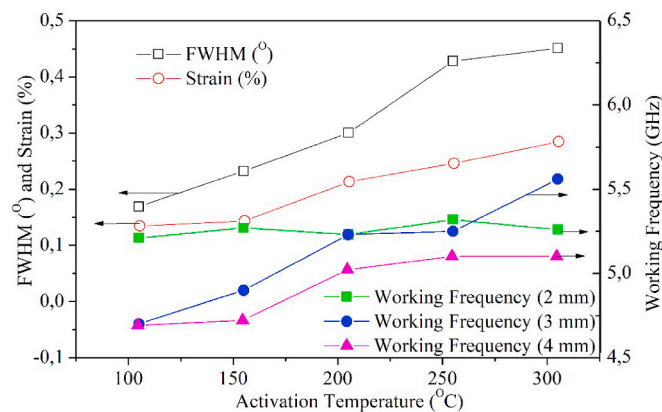


Fig. 7. Relation between FWHM and strain values from the quantitative analysis of XRD spectrum of Fe/CNs/PVA nanocomposites for various activation temperature with working frequency for various thickness as function of activation temperature.

method. The CNs are useful for attaching the Fe particles and play a role in reducing the magnetic properties of nanocomposites. The distance ( $\Delta(\text{LO-TO})$ ) between two optical phonon vibrations is  $120 \text{ cm}^{-1}$  for the  $305^\circ\text{C}$  of the activation temperature with the thickness 4 mm indicated stable covalent bonding formation with a new structure was formed. The thickness and the distance ( $\Delta(\text{LO-TO})$ ) is an essential parameter for increasing the reflection loss and the electromagnetic waves absorption level. The activation temperature of CNs influences RL and frequency. The highest RL is  $-23.64 \text{ dB}$  for activation temperature at  $305^\circ\text{C}$  potentials to attenuate 99% of EM wave for the working frequency at 5.56 GHz indicated that nano-composite in this study has a high potential for a new type of EM wave absorber.

#### CRedit authorship contribution statement

**Yulia Kirana Lahsmin:** Conceptualization, Methodology, Visualization, Investigation. **Heryanto Heryanto:** Data analysis, Writing - original draft. **Sultan Ilyas:** Formal analysis, Writing - original draft. **Ahmad Nurul Fahri:** Visualization, Investigation. **Bualkar Abdullah:** Supervision, Validation. **Dahlang Tahir:** Supervision, Validation, Writing - review & editing.

#### Declaration of competing interest

The authors declare that they have no known competing financial interests or personal relationships that could have appeared to influence the work reported in this paper.

#### Acknowledgments

This work was supported by the PTM (Penelitian Tesis Magister) funded by the Government of Indonesia (Kemenristek/BRIN) grants: 1517/UN4.22/PT.01.03/2020.

#### References

- [1] B. Abdullah, S. Ilyas, D. Tahir, Nano-composite Fe/activated carbon/PVA for microwave absorber: synthesis and characterization, *J. Nanomater.* 6 (2018) 9823263.
- [2] B. Qiu, C.L. Zhu, C.Y. Li, X.T. Zhang, Y.J. Chen, Coupling hollow  $\text{Fe}_3\text{O}_4$ -Fe nanoparticles with graphene sheets for high-performance electromagnetic wave absorbing material, *ACS Appl. Mater. Interfaces* 8 (2016) 3730–3735.
- [3] L. Wang, H. Guan, J. Hu, C. Dong, Y. Wang,  $\text{Fe}_3\text{O}_4/\text{Fe}/\text{C}$  composites prepared by a facile thermal decomposition method and their application as microwave absorbers, *J. Allowance Comp.* 784 (2019) 1123–1129.
- [4] T. Wu, Y. Liu, X. Zeng, T.T. Cui, Y.T. Zhao, Y.N. Li, G.X. Tong, Facile hydrothermal synthesis of  $\text{Fe}_3\text{O}_4/\text{C}$  core-shell nanorings for efficient low-frequency microwave absorption, *ACS Appl. Mater. Interfaces* 8 (2016) 7370–7380.

- [5] S.S. Kim, S.T. Kim, J.M. Ahn, K.H. Kim, Magnetic and microwave absorbing properties of Co-Fe thin films plated on hollow ceramic microspheres of low density, *J. Magn. Magn. Mater.* 271 (2014) 39–45.
- [6] Q. Liu, X. Liu, H. Feng, H. Shui, R. Yu, Metal organic framework-derived Fe/carbon porous composite with low Fe content for lightweight and highly efficient electromagnetic wave absorber, *Chem. Eng. J.* 314 (2017) 320–327.
- [7] D. Tahir, S. Ilyas, B. Abdullah, B. Arminyah, K. Kim, H.J. Kang, Modification in electronic, structural, and magnetic properties based on composition of composites Copper (II) Oxide (CuO) and Carbonaceous material, *Mater. Res. Express* 6 (2019), 035705.
- [8] K. Zhang, X. Gao, Q. Zhang, T. Li, H. Chen, X. Chen, Preparation and microwave absorption properties of asphalt carbon coated reduced graphene oxide/magnetic  $\text{COFe}_2\text{O}_4$  hollow particles modified multi-walled carbon nanotube composites, *J. Alloys Compd.* 723 (2017) 912–921.
- [9] D. Tahir, S. Ilyas, B. Abdullah, B. Arminyah, H.J. Kang, Electronic properties of composites iron (II,III) oxide ( $\text{Fe}_3\text{O}_4$ ) carbonaceous absorber materials by electron spectroscopy, *J. Electron. Spectrosc. Relat. Phenom.* 229 (2018) 47–51.
- [10] B. Abdullah, A. Nisyah, S. Ilyas, D. Tahir, Structural properties and bonding characteristics of honeycomb structure of composite  $\text{ZnMnO}_2$  and activated carbon, *J. Appl. Biomater. Funct. Mater.* 17 (2019) 1–6.
- [11] Abdullah B. Hendri, D. Tahir, S. Fatimah, New types composite copper (Cu) and activated carbon (C) for electromagnetic wave absorber materials, *J. Phys. Conf.* 1242 (2019), 012031.
- [12] J. Fang, T. Liu, Z. Chen, Y. Wang, W. Wei, X. Yue, Z.A. Jiang, Wormhole-like porous carbon/magnetic particles composite as an efficient broad band electromagnetic wave absorber, *Nanoscale* 8 (2016) 8999–8999.
- [13] R. Kuchi, M. Sharma, S.W. Lee, D. Kim, J.R. Jeong, N. Jung, Rational design of carbon shell-encapsulated cobalt nanospheres to enhance microwave absorption performance, *Prog. Nat. Sci.: Mater. Int.* 29 (2019) 88–93.
- [14] C. Zhou, S. Geng, X. Xu, T. Wang, L. Zhang, X. Tian, F. Yang, H. Yang, Y. Li, Lightweight hollow carbon nanospheres with tunable sizes towards enhancement in microwave absorption, *Carbon* 108 (2016) 234–241.
- [15] H.J. Yang, W.Q. Cao, D.Q. Zhang, T.J. Su, H.L. Shi, W.Z. Wang, J. Yuan, M.S. Cao, NiO hierarchical nanorings on SiC: enhancing relaxation to tune microwave absorption at elevated temperature, *ACS Appl. Mater. Interfaces* 7 (2016) 7073–7077.
- [16] H. Zhang, L. Quan, L. Xu, Effects of amino-functionalized carbon nanotubes on the crystal structure and thermal properties of polyacrylonitrile homopolymer microspheres, *Polymers* 9 (2017) 332.
- [17] A.S. Hoang, Electrical conductivity and electromagnetic interference shielding characteristics of multiwalled carbon nanotube filled polyurethane composite films, *Adv. Nat. Sci. Nanosci. Nanotechnol.* 2 (2011), 025007.
- [18] D. Tahir, J. Krauer, S. Tougaard, Electronic and optical properties of Fe, Pd, and Ti studied by reflection electron energy loss spectroscopy, *J. Appl. Phys.* 115 (2014) 243508.
- [19] D. Tahir, S.K. Oh, H.J. Kang, S. Tougaard, Quantitative analysis of reflection electron energy loss spectra to determine electronic and optical properties of Fe-Ni alloy thin films, *J. Electron. Spectrosc. Relat. Phenom.* 206 (2016) 6–11.
- [20] S. Kaassamani, W. Kassem, M. Tabbal, X-ray diffraction line shape analysis of pulsed laser deposited ZnO nanostructured thin films, *Appl. Surf. Sci.* 473 (2019) 298–302.
- [21] L. Xiaohui, M. Zengming, Q.J.Z. Bin, G. Weihua, Z. Zhu, J. Guangbin, Environment-stable  $\text{Co}_3\text{Ni}_2$  encapsulation in stacked porous carbon nanosheets for enhanced microwave absorption, *Nano-Micro Lett.* 12 (2020) 102.
- [22] L. Xiaohui, Q. Bin, M. Zengming, C. Bingchen, L. Nan, W. Chenhao, J. Guangbin, Y. Ting, Self-assembly three-dimensional porous carbon networks for efficient dielectric attenuation, *ACS Appl. Mater. Interfaces* 11 (33) (2019) 30228–30233.
- [23] C. Yan, Z.Y.S. Justin, Z. Huanqin, J.X. Zhichuan, J. Guangbin, A flexible and lightweight biomass-reinforced microwave absorber, *Nano-Micro Lett.* 12 (2020) 125.
- [24] L. Wei, T. Shujuan, Y. Zhihong, J. Guangbin, Enhanced low-frequency electromagnetic properties of MOF-derived cobalt through interface design, *ACS Appl. Mater. Interfaces* 10 (37) (2018) 31610–31622.
- [25] Y.K. Lahsmin, D. Tahir, B. Abdullah, S. Ilyas, I. Mutmainna, Synthesis of carbon nanosphere at low temperatures based on bamboo fiber, *Mater. Sci. Forum* 966 (2019) 163–168.
- [26] M.H. Makied, E. Sheha, T.S. Shanap, M.K. El-Mansy, Electrical conduction and dielectric relaxation in p-type PVA/Cul polymer composite, *J. Adv. Res.* 4 (2013) 531–538.
- [27] A.Y. Yassin, Dielectric spectroscopy characterization of relaxation in composite based on (PVA-PVP) blend for nickel-cadmium batteries, *J. Mater. Sci. Mater. Electron.* (2020), <https://doi.org/10.1007/s10854-020-04478-1>.
- [28] D. Tahir, S.K. Oh, H.J. Kang, S. Tougaard, Composition dependence of dielectric and optical properties of HF-Zr-silicate thin films grown on Si (100) by atomic layer deposition, *Thin Solid Films* 616 (2016) 425–430.
- [29] S. Heo, D. Tahir, J.G. Chung, J.C. Lee, K.H. Kim, J. Lee, H.I. Lee, G.S. Park, S.K. Oh, H.J. Kang, P. Choi, B.D. Choi, Band alignment of atomic layer deposited ( $\text{HFZrO}_4$ ) $_x$ ( $\text{SiO}_2$ ) $_y$  gate dielectrics on Si (100), *Appl. Phys. Lett.* 107 (2015) 182101.
- [30] D. Tahir, Suarga, N.H. Sari, Yulianti, Stopping powers and inelastic mean free path of 200 eV–50 keV electrons in polymer PMMA, PE, and PVC, *Appl. Radiat. Isot.* 95 (2015) 59–62.
- [31] D. Tahir, E.H. Choi, Y.J. Cho, S.K. Oh, H.J. Kang, H. Jin, S. Heo, J.G. Chung, J. C. Lee, S. Tougaard, Electronic and optical properties of La-aluminate dielectric thin films on Si (100), *Surf. Interface Anal.* 42 (10–11) (2010) 1566–1569.

- [32] S. Ilyas, B. Abdullah, D. Tahir, Enhancement of absorbing frequency and photocatalytic performance by temperature treatment of composites Fe<sub>3</sub>O<sub>4</sub>-AC nanoparticle, *Adv. Powder Technol.* 31 (3) (2020) 905–913.
- [33] S. Suryani, Tahir D. Heryanto, Stopping Powers and inelastic mean free path from quantitative analysis of experimental REELS spectra for electrons in Te, Fe, Ni, and Pd, *Surf. Interface Anal.* 52 (2019) 1–7.
- [34] S. Suryani, H. Heryanto, R. Rusdaeni, A.N. Fahri, D. Tahir, Quantitative analysis of diffraction and infra-red spectra of composite cement/BaSO<sub>4</sub>/Fe<sub>3</sub>O<sub>4</sub> for determining correlation between attenuation coefficient, structural and optical properties, *Ceram. Int.* 46 (2020) 18601–18607.
- [35] M. Ghasemifard, S.M. Hosseini, Khorami GhH, Synthesis and Structure of PMN-PT ceramic nanopowder free from pyrochlore phase, *Ceram. Int.* 35 (2009) 2899–2905.
- [36] L. Legana, T. Leskovaar, M. Cresnar, F. Cavalli, D. Innocenti, P. Ropret, Non-invasive reflection FTIR characterization of archaeological burnt bones: reference database and case studies, *J. Cult. Herit.* 41 (2019) 13–26.
- [37] Khorami GhH, A.K. Zak, A. Kompany, R. Yousefi, Optical and structural properties of X-doped (X = Mn, Mg, and Zn) PZT nanoparticles by Kramers–Kronig and size strain plot methods, *Ceram. Int.* 38 (2012) 5683–5690.
- [38] M. Nadafan, M.R. Tohidifar, M. Karimi, R. Malekfar, G. Khorrami, Assessment of the optical and dielectric properties of f-MWCNTs/BaTiO<sub>3</sub> nanocomposite ceramics, *Ceram. Int.* 44 (13) (2018) 15804–15808.
- [39] M. Nadafan, M.R. Tohidifar, Evaluation of structural, optical and dielectric properties of MWCNT-BaTiO<sub>3</sub>/silica ceramic nanocomposites, *Ceram. Int.* 26 (8) (2020) 12243–12248.
- [40] X. Lu, J. Chen, M. Zheng, J. Guo, J. Qi, Y. Chen, S. Miao, B. Zheng, Effect of high-intensity ultrasound irradiation on the stability and structural features of coconut-grain milk composite system utilizing maize kernels and starch with different amylose contents, *Ultrason. Sonochem.* 55 (2019) 135–148.
- [41] M. Ghasemifard, E. Fathi, M. Ghamari, The effect of Fe<sup>3+</sup>-doped on structure and optical properties of mesoporous Al<sub>2</sub>O<sub>3</sub>/SiO<sub>2</sub> composite, *Mater. Sci. Semicond. Process.* 42 (2016) 349–353.
- [42] Z. Yang, Z. Li, T. Ning, M. Zhang, Y. Yan, D. Zhang, G. Cao, Microwave dielectric properties of B and N co-doped SiC nanopowders prepared by combustion synthesis, *J. Alloys Compd.* 777 (2019) 1039–1043.
- [43] K. Praveena, K. Sadhana, H.L. Liu, N. Maramu, G. Himanandini, Improved microwave absorption properties of TiO<sub>2</sub> and Ni<sub>0.53</sub>Cu<sub>0.12</sub>Zn<sub>0.35</sub>Fe<sub>2</sub>O<sub>4</sub> nanocomposites potential for microwave devices, *J. Alloys Compd.* 681 (2016) 499–507.
- [44] Y. Zhang, Y. Huang, H. Chen, Z. Huang, Y. Yang, P. Xiao, Y. Zhou, Y. Chen, Composition and structure control of ultralight graphene foam for high-performance microwave absorption, *Carbon* 105 (2016) 438–447.
- [45] P. Liu, Y. Huang, J. Yan, Y. Zhao, Magnetic graphene@PANI@porous TiO<sub>2</sub> ternary composites for high-performance electromagnetic wave absorption, *J. Mater. Chem.* 4 (2016) 6362–6370.
- [46] J. Li, Y. Xie, W. Lu, T.W. Chou, Flexible electromagnetic wave absorbing composite based on 3D rGO-CNT-Fe<sub>3</sub>O<sub>4</sub> ternary films, *Carbon* 129 (2018) 76–84.
- [47] R. Zhang, X. Huang, B. Zhong, L. Xia, G dan Wen, Y. Zhou, Enhanced microwave absorption properties of ferroferric oxide/graphene composites with a controllable microstructure, *RSC Adv.* 6 (2016) 16952–16962.
- [48] B. Zhang, C. Lu, H. Lu, Improving microwave adsorption property of ZnO particle by doping graphene, *Mater. Lett.* 116 (2014) 16–19.
- [49] H. Lv, Y. Guo, Y. Zhao, H. Zhang, B. Zhang, G. Ji, Z.J. Xu, Achieving tunable electromagnetic absorber via graphene/carbon sphere composites, *Carbon* 110 (2016) 130–137.
- [50] A. Olad, S. Shakoori, Electromagnetic interference attenuation and shielding effect of quaternary Epoxy-PPy/Fe<sub>3</sub>O<sub>4</sub>-ZnO nanocomposite as a broad band microwave-absorber, *J. Magn. Magn Mater.* 458 (2018) 335–345.
- [51] Y. Qing, W. Zhou, F. Luo, D. Zhu, Titanium carbide (MXene) nanosheets as promising microwave absorbers, *Ceram. Int.* 42 (2016) 16412–16416.
- [52] L. Quan, F.X. Qin, D. Esteves, H. Wang, H.X. Peng, Magnetic graphene for microwave absorbing application: toward the lightest graphene-based absorber, *Carbon* 125 (2017) 630–639.
- [53] F. Ren, Z. Guo, Y. Shi, L. Jia, Y. Qing, P. Ren, D. Yan, Lightweight and highly efficient electromagnetic wave-absorbing of 3D CNTs/GNS@CoFe<sub>2</sub>O<sub>4</sub> ternary composite aerogels, *J. Alloys Compd.* 768 (2018) 6–14.
- [54] H. Wang, L. Xiang, W. Wei, J. An, J. He, C. Gong, Y. Hou, Efficient and lightweight electromagnetic wave absorber derived from metal organic framework-encapsulated cobalt nanoparticles, *Applied Materials and Interfaces* 9 (2017) 42102–42110.
- [55] S. Wei-li, C. Mao-sheng, H. Zhi-ling, Y. Jie, F. Xiao-yong, High-temperature microwave absorption and evolutionary behavior of multiwalled carbon nanotube nanocomposite, *Scripta Mater.* 61 (2) (2009) 201–204.
- [56] Z. Qian, Y. Xiaowei, Y. Fang, T. Zhiming, M. Ran, C. Laifei, High temperature electromagnetic wave absorption properties of SiC<sub>f</sub>/Si<sub>3</sub>N<sub>4</sub> composite induced by different SiC fibers, *Ceram. Int.* 45 (5) (2019) 6514–6522.
- [57] W. Bo, C. Mao-Sheng, H. Zhi-Ling, S. Wei-Li, Z. Lu, L. Ming-Ming, J. Hai-Bo, F. Xiao-Yong, W. Wen-Zhong, Y. Jie, Temperature dependent microwave attenuation behavior for carbon-nanotube/silica composites, *Carbon* 65 (2013) 124–139.